Atmos. Chem. Phys. Discuss., 14, 23027–23073, 2014
www.atmos-chem-phys-discuss.net/14/23027/2014/
doi:10.5194/acpd-14-23027-2014

Atmospheric Chemistry and Physics Discussions

Single-particle characterization of ice-nucleating particles and ice particle residuals sampled by three different techniques

A. Worringen[1,6], K. Kandler[1], N. Benker[1], T. Dirsch[1], S. Weinbruch[1], S. Mertes[2], L. Schenk[2], U. Kästner[2], F. Frank[3], B. Nillius[3,5], U. Bundke[3,*], D. Rose[3], J. Curtius[3], P. Kupiszewski[4], E. Weingartner[4,], J. Schneider[5], S. Schmidt[5], and M. Ebert[1]**

[1]Institut für Angewandte Geowissenschaften, Technische Universität Darmstadt, Schnittspahnstr. 9, 64287 Darmstadt, Germany
[2]Leibniz-Institut für Troposphärenforschung, Permoserstraße 15, 04318 Leipzig, Germany
[3]Institut für Atmosphäre und Umwelt, Goethe-Universität Frankfurt am Main, Altenhöferallee 1, 60438 Frankfurt am Main, Germany
[4]Laboratory of Atmospheric Chemistry, Paul Scherrer Institute, 5232 Villigen PSI, Switzerland
[5]Max-Planck-Institut für Chemie, Hahn-Meitner-Weg 1, 55128 Mainz, Germany
[6]Institut für Physik der Atmosphäre, Johannes Gutenberg Universität Mainz, 55099 Mainz, Germany

*now at: Forschungszentrum Juelich GmbH, 52425 Jülich, Germany
**now at: University of Applied Sciences and Arts Northwestern Switzerland, School of Engineering, Institute of Aerosol and Sensor Technology, Klosterzelgstrasse 2, 5210 Windisch, Switzerland

Received: 14 August 2014 – Accepted: 20 August 2014 – Published: 8 September 2014

Correspondence to: A. Worringen (worr@geo.tu-darmstadt.de)

Published by Copernicus Publications on behalf of the European Geosciences Union.

ACPD
14, 23027–23073, 2014

Abstract

In the present work, three different techniques are used to separate ice-nucleating particles (INP) and ice particle residuals (IPR) from non-ice-active particles: the Ice Selective Inlet (ISI) and the Ice Counterflow Virtual Impactor (Ice-CVI), which sample ice particles from mixed phase clouds and allow for the analysis of the residuals, as well as the combination of the Fast Ice Nucleus Chamber (FINCH) and the Ice Nuclei Pumped Virtual Impactor (IN-PCVI), which provides ice-activating conditions to aerosol particles and extracts the activated ones for analysis. The collected particles were analyzed by scanning electron microscopy and energy-dispersive X-ray microanalysis to determine their size, chemical composition and mixing state. Samples were taken during January/February 2013 at the High Alpine Research Station Jungfraujoch. All INP/IPR-separating techniques had considerable abundances (median 20–70 %) of contamination artifacts (ISI: Si-O spheres, probably calibration aerosol; Ice-CVI: Al-O particles; FINCH + IN-PCVI: steel particles). Also, potential measurement artifacts (soluble material) occurred (median abundance < 20 %). After removal of the contamination particles, silicates and Ca-rich particles, carbonaceous material and metal oxides were the major INP/IPR particle types separated by all three techniques. Minor types include soot and Pb-bearing particles. Sea-salt and sulfates were identified by all three methods as INP/IPR. Lead was identified in less than 10 % of the INP/IPR. It was mainly present as an internal mixture with other particle types, but also external lead-rich particles were found. Most samples showed a maximum of the INP/IPR size distribution at 400 nm geometric diameter. In a few cases, a second super-micron maximum was identified. Soot/carbonaceous material and metal oxides were present mainly in the submicron range. ISI and FINCH yielded silicates and Ca-rich particles mainly with diameters above 1 µm, while the Ice-CVI also sampled many submicron particles. Probably owing to the different meteorological conditions, the INP/IPR composition was highly variable on a sample to sample basis. Thus, some part of the discrepancies between the different techniques may result from the (unavoidable) non-parallel sampling.

ACPD
14, 23027–23073, 2014

The observed differences of the particles group abundances as well as the mixing state of INP/IPR point to the need of further studies to better understand the influence of the separating techniques on the INP/IPR chemical composition.

1 Introduction

The impact of clouds – and in particular cloud-aerosol interactions – on the earth's radiation balance is still one of the most uncertain aspects in our understanding of the climate system (Flato et al., 2013). The understanding of tropospheric cloud ice formation processes is crucial for predicting precipitation and cloud radiative properties. Aerosol-cloud interactions play a key role in determining cloud properties like phase, size distribution and colloidal stability of the cloud elements, as well as the lifetime, dimensions and precipitating efficiency of the cloud. Though there has been an advance during the last decades, in particular for aerosol-cloud-interactions, the level of scientific understanding is still classified as "very low" to "low" (Flato et al., 2013). A considerable uncertainty of the response of aerosol and cloud processes to changes in aerosol properties still arises from the lack of fundamental understanding of the interaction of aerosol particles with the cloud ice phase (Lohmann and Feichter, 2005). One particular problem in understanding the INP properties of atmospheric aerosol is the small data base of field measurements.

Many ice nucleation experiments were performed under laboratory conditions (e.g., Hoose and Möhler, 2012), and provided knowledge on principle INP properties of pure components and artificially generated mixtures. Mineral dust and biological particles are regarded in general as efficient INP, while experiments disagreed on the INP abilities of soot and organics (Hoose and Möhler, 2012). Sea-salt and sulfate are usually not considered as INP. However, it was shown recently for NaCl particles that a partial efflorescence under suitable conditions might lead to NaCl ice activation (Wise et al., 2012). The situation is more complex in the ambient atmosphere, where particles are usually present as a mixture of different compounds and get modified by

ACPD
14, 23027–23073, 2014

heterogeneous processes, which may then lead to modified INP properties. In laboratory experiments, these effects are currently addressed for single substances (Hoose and Möhler, 2012; Wex et al., 2014), but the level of atmospheric mixing complexity is not yet reached. Therefore, field measurements are highly needed.

Several techniques emerged in particular during the last decade, which are capable to provide selectively sampled INP or IPR for further chemical analysis. Techniques measuring the INP ability of aerosol particles usually expose a sampled aerosol to thermodynamic conditions favoring ice nucleation, after which the activated particles are separated from the non-activated ones. Examples of these techniques are the Fast Ice Nucleus Chamber (FINCH) (Bundke et al., 2008) in combination with the IN- pumped counterflow virtual impactor (IN-PCVI) (Schenk, 2014) and the Frankfurt Ice Nuclei Deposition Freezing Experiment (FRIDGE) (Klein et al., 2010; Bundke et al., 2008). While in FINCH the particles are kept airborne, ice nucleation occurs on an ice-inert substrate in FRIDGE. In contrast, analysis of IPR relies on the natural selection of INP by a cloud. While for cirrus clouds all cloud elements can be investigated (Cziczo and Froyd, 2014), for mixed phase clouds the ice particles need to be separated from droplets. Ice particle separation is currently done either by the Bergeron–Findeisen process, whereby droplets present in the sample flow are evaporated in an ice-saturated environment, with an Ice Selective Inlet (P. Kupiszeski et al., personal communication, 2014) and subsequent selection of the larger cloud elements with a pumped counterflow virtual impactor. Alternatively, cloud elements are impacted on a cooled surface collecting the droplets while bouncing the ice particles for further analysis (Ice-CVI) (Mertes et al., 2007).

In the present work, three state-of-the-art techniques for INP/IPR sampling – ISI, Ice-CVI and FINCH + IN-PCVI – were operated in parallel in a joint field experiment to sample atmospheric mixed-phase clouds and characterize the sampled INP/IPR with respect to their morphology, chemical composition, particle size and particle mixing state.

ACPD
14, 23027–23073, 2014

2 Experimental

In January/February 2013, a field campaign of INUIT (Ice Nuclei Research Unit) was performed at the High Alpine Research Station Jungfraujoch in Switzerland (JFJ, 3580 m a.s.l., 46.55° N, 7.98° E), as part of the Cloud and Aerosol Characterization Experiment (CLACE) 2013. Ice-nucleating particles (INP) and ice particle residuals (IPR), separated from the interstitial aerosol and droplets by ISI and Ice-CVI and from the total aerosl by FINCH + IN-PCVI (Table 1), were collected by impactors and analyzed by scanning electron microscopy (SEM) and energy-dispersive X-ray microanalysis (EDX). In addition, the INP/IPR were analyzed by laser ablation mass spectrometry (LA-MS).

2.1 INP/IPR differentiation

INP were detected by the FINCH + IN-PCVI (Bundke et al., 2008). The atmospheric aerosol particles were sampled by a total aerosol inlet (Weingartner et al., 1999) and transported into FINCH + IN-PCVI.

IPR were collected via selective sampling of small (< 20 µm aerodynamic diameter) ice crystals with ICE-CVI and ISI, and subsequent heating of the sampled crystals (resulting in release of the IPR). The extracted IPR were collected with a two-stage impactor system (see above).

For the scanning electron microscopy analysis the released INP were collected by a two-stage impactor using circular nozzles of 0.7 and 0.25 mm at a flow rate of 7.5 $cm^3 s^{-1}$ (volume), leading to approximate 50 % cut-off efficiency aerodynamic diameters of 1 and 0.1 µm, respectively (for details on impactor dimensions see Kandler et al., 2007). Transmission electron microscopy grids (type S162N9, Plano GmbH, Wetzlar, Germany) and polished elemental boron embedded in a conductive resin were used as impaction substrates.

ACPD
14, 23027–23073, 2014

2.1.1 Coupling of FINCH and IN-PCVI

Aerosol particles were sampled from the atmosphere by a total aerosol inlet (Weingartner et al., 1999) and transported into FINCH, in which a supersaturation with respect to ice is achieved by mixing air flows with different temperature and humidity. Ice nucleating particles are activated, grow while flowing through the chamber, and are counted in an optical particle counter (OPC). The OPC used in this instrument is able to distinguish between supercooled water droplets and ice crystals by analyzing the polarization ratio of the scattered circular polarized light (P44/P11 ratio of the scattering matrix; Hu et al., 2003). Also, the auto-fluorescence resulting from the excitation of the grown particles with UV light is detected (Bundke et al., 2010), which is an indication for biological particle material.

In a second step, particles that had grown to ice crystals were separated (IN-PCVI) (Schenk et al., 2014) from the remaining non-activated and therefore hardly grown aerosol particles and small supercooled droplets. This is realized by a counterflow that meets the FINCH output flow which is at the same time the IN-PCVI input flow. During the INUIT-JFJ 2013 campaign the adjusted counterflow to input flow ranges leads to cut off diameters between 4.5–8 µm. The sampled FINCH ice particles evaporate while they are transported in a dry particle free air flow within the IN-PCVI.

During INUIT-JFJ 2014, FINCH + IN-PCVI was connected to a total aerosol inlet and sampled approximately 2.25 $\mathrm{L\,min^{-1}}$ aerosol flow. Supersaturation and freezing temperature were varied during the campaign.

2.1.2 Ice-CVI

From the mixed-phase clouds prevailing at JFJ, the ice particle residuals were collected by the so-called Ice-CVI (Mertes et al., 2007). It consists of a series of different modules that allow the sampling of small ice particles by a simultaneous pre-segregation of all other cloud constituents. The vertical, omni-directional inlet already reduces the sampling of ice crystals larger than 50 µm, including precipitating or windblown ice particles.

ACPD
14, 23027–23073, 2014

A virtual impactor downstream the inlet horn limits the upper size of sampled hydrometeors to 20 µm. This limit is reasonable, because the collection efficiency is nearly 1 for these ice particle sizes. The ice particle break-up is minimized in the subsequent Ice-CVI components, and ice particles in this size range grow by water vapour diffusion, i.e. they should contain only the former INP as a residual particle. Downstream of the virtual impactor a pre-impactor removes supercooled drops by contact freezing on cold impaction plates. Ice particles bounce and pass the impaction plates. A conventional CVI (Mertes et al., 2005a, b) is located downstream of the pre-impactor to reject interstitial particles smaller than 5 µm. Thus, only ice particles in the 5–20 µm diameter range completely traverse the Ice-CVI. As with a conventional CVI these small ice crystals are injected into a particle-free and dry carrier gas which leads to evaporation and allows the analysis of the ice particle residues.

2.1.3 Ice Selective Inlet (ISI)

The novel Ice Selective Inlet (ISI) was designed to extract small ice crystals from mixed-phase clouds, simultaneously counting, sizing and imaging the hydrometeors contained in the cloud with the use of WELAS (white light aerosol spectrometers) 2500 sensors and a Particle Phase Discriminator (PPD-2K). The core of ISI is a droplet evaporation unit with ice-covered inner walls, removing droplets using the Bergeron–Findeisen process, while transmitting the ice crystals. In the final stage of ISI, a pumped counterflow virtual impactor removes interstitials and cloud condensation nuclei released in the droplet evaporation unit from the sample flow, thus ensuring only ice crystals are transmitted. The extracted ice crystals are subsequently sublimated, releasing the ice particle residuals (IPR), which are transferred into the laboratory for further on- and offline characterization of their physical and chemical properties.

ACPD
14, 23027–23073, 2014

2.1.4 Laser Ablation Spectrometry (LA-MS)

The deployed laser ablation aerosol spectrometer was the ALABAMA (Aircarft-based Laser Ablation Aerosol Mass Spectrometer) which was originally developed for aircraft operation at MPIC (Brands et al., 2011), but has since also then been used in several ground-based measurement projects. It provides the chemical composition of single aerosol particles in an aerodynamic particle size range between 150 and 1500 nm, including refractory compounds such as metals, dust, and soot. It was used during the INUIT-JFJ campaign for the analysis of background aerosol particles and IPR (Schmidt et al., 2014). The IPR were sampled through the Ice-CVI (1663 mass spectra during 104 h) and through the ISI (146 mass spectra in 32 h).

2.2 Sample analysis by electron microscopy

Forty six samples were acquired during the field campaign. All samples were analyzed by scanning electron microscopy (FEI Quanta 200 FEG, FEI, Eindhoven, the Netherlands) and energy-dispersive X-ray microanalysis (EDX, EDAX, Tilburg, the Netherlands). The particles were manually characterized with respect to their chemical composition, size, morphology, internal mixing state and stability under electron bombardment. Particle size was determined as average geometrical diameter from the electron images. In addition, automated particles analysis controlled by the software Genesis 5.11 (AMETEK, Wiesbaden, Germany) was performed. Results from the automated analysis were classified based on the chemical composition of the particles only (Scheuvens et al., 2011).

2.3 Particle classification

Based on chemical composition, morphology mixing state and beam stability, 18 particle classes were defined and combined into 11 particles classes. Table 2 lists the particle groups, particle classes and classification criteria for the manual analysis.

ACPD
14, 23027–23073, 2014

Pb-bearing particles are classified according to the presence of Pb only. They might be homogeneous Pb-rich particles or particles containing Pb-rich inclusions. In the latter case, the main matrix particles can be carbonaceous, soot, sulfate, sea-salt, silicate, metal oxide, a droplet or belong to the "other" class. Droplets are identified by their typical morphology of larger residual particles centered in a halo of small residuals, originating from the splashing of the droplet at impaction. The center of the residual can consist of unstable (e.g. sulfate) or stable sea-salt, silicate, metal oxide, Ca-rich particles, or mixtures thereof. The halo particles are usually unstable under electron bombardment. Particles which could not be classified according to the criteria are summarized in the particle class "other". This particle class includes Zn-rich, Mg-rich particles as well as Sn-, Ba-, Bi- and Br-bearing particles.

The automated particle analysis does not yield suitable information on particle morphology. Thus, carbonaceous and soot particles cannot be distinguished. In addition, droplets are not recognized by automated analysis. Therefore, the morphology information was obtained by manual analysis in all samples, except for one sample of total aerosol. In this one sample, residues of droplets are classified as sea-salt, silicate with coating, metal oxide with coating, Ca-rich particle with coating or as unstable sulfate.

Due to the difference in sample substrate composition between TEM grids and elemental boron, in particular for the detection of carbonaceous particles and thin carbonaceous coatings, systematic deviations can occur with a bias towards better detection of these particles on boron.

2.4 Sampling location and meteorology

The JFJ station is located in a saddle between the mountains Jungfrau and Mönch, which is oriented WSW – NNE. This topography results in a channeling of the atmospheric flow leading to a near-binary distribution of wind directions as either NW or SSE. The atmospheric conditions during the campaign are illustrated in Fig. 1. Hourly 5 day backward trajectories for the JFJ station were calculated with the HYSPLIT model based on GDAS data (Draxler and Rolph, 2013).

ACPD
14, 23027–23073, 2014

At the top of Fig. 1, periods with comparatively homogeneous atmospheric conditions during which samples using different techniques are marked. Homogeneity was determined from meteorology, particle concentrations and changes in air mass provenance. Details are given for period A, as samples are compared below for this time period.

Period A: 2 February/13:00–18:00 (UTC): air mass backward trajectories cross France at an altitude of 0.5 km for about half a day, and the northwestern tip of Spain for a few hours. For the rest of the 4.5 days trajectory length, the air masses were in the free troposphere over the Atlantic Ocean west and southwest of France and Spain. Wind, temperature and in-cloud conditions were very stable during this period. While the JFJ is usually in the free troposphere during the winter months (Collaud Coen et al., 2011), abrupt increases in particle concentrations may indicate a rise in the atmospheric boundary layer height to the station altitude which leads to a local influence. This effect is visible as a sudden increase in particle concentration in the middle of this period. We consider period A as of Atlantic/free-troposphere origin with minor local influence.

3 Results

3.1 Artifact particles

3.1.1 Contamination artifact particles from the INP/IPR sampling instruments

The sampling instruments yielded different types of artifact particles indicated by their clear non-atmospheric origin. Therefore, they were removed from further analysis. Figure 2 shows secondary electron images of the most common contamination artifact particles and their energy-dispersive X-ray spectra. The relative abundance of the dominating artifact particles for each instrument is shown in Fig. 3.

ACPD
14, 23027–23073, 2014

With all three sampling techniques, minor amounts of Fe-Cr particles are observed as an artifact. They may derive from internal abrasion of the instrument or tubing. For the samples collected on boron substrates, in addition Cu-rich particles are present as artifacts, which fragment from the embedding material of the boron substrates.

In the ISI samples, mainly Si-O spheres with a size of approx. 1 µm are observed as artifacts. These particles were most likely introduced into the instrument during calibration of the optical particle spectrometers contained within the inlet. The abundance of Si-O spheres in the samples ranged from 26 to 94 %. Including the Fe-Cr-rich and Cu-rich artifacts, the abundance of all artifact particles ranged from 46 to 94 % during the measurement period.

In the FINCH + IN-PCVI samples, Fe-Cr-rich and Cu-rich particles as well as a few Au/Ag particles (not shown as image) were identified as instrumental artifact. Their abundance ranged from 12 to 60 % with a median of 20 %.

In the Ice-CVI samples, Al-O particles – probably aluminium oxides/hydroxides – occur as artifact particles originating most likely from the impaction plates. The relative abundance of these Al-O particles varied in the range of 10–94 %. As all Al-O particles are classified as artifacts in the present paper, potentially occurring atmospheric aluminium oxides/hydroxide particles in the Ice-CVI would be overlooked. However, it can be safely assumed that this potential error is minor, as no Al-O particles with the characteristic morphology (Fig. 2) were identified with the other two sampling instruments. The abundance of other artifact particles in the Ice-CVI sample is small (range of 0–8 %).

In summary, it must be concluded that the abundance of contamination artifacts in the separated INP and IPR is generally large and cannot be neglected. Thus, the INP/IPR concentrations must be corrected to obtain accurate results. It is highly recommended that measurements of INP/IPR concentrations are always accompanied by chemical and morphological single particle characterization in order to avoid large systematic errors caused by contamination artifacts.

ACPD
14, 23027–23073, 2014

3.1.2 Potential INP/IPR sampling artifacts

In addition to contamination artifacts, INP/IPR sampling artifacts seem to occur. We define sampling artifacts as particles which pass the selection mechanisms similar to INP/IPR, but are not expected to act as INP/IPR. The potential sampling artifacts include sea-salt particles, sulfate particles and particles which impact on the sampling substrates as droplets. As we cannot exclude that these particles may have acted as INP/IPR, we do not exclude them from further analysis in contrast to the contamination artifacts.

Droplets are characterized by their morphology of a residue with a halo (Fig. 4). While in principle the heating and drying line should lead to total evaporation of particle-bound water, obviously some particles were still in liquid state during impaction sampling. As we cannot distinguish incompletely dried ice residuals from super-cooled droplets, which were falsely identified as INP/IPR, we consider droplets as artifacts. This is supported by the fact that the droplet residuals were composed either mainly of sulfate or the residuals were volatile, neither of these residual types are expected to be efficient INP/IPR.

As expected, the sulfate particles were preferentially found in the submicron size range, while sea-salt particles have a tendency to be of larger sizes. Droplets, however, occur rather uniformly in sub-/supermicron sizes.

The relative number abundance of the three potential sampling artifacts (droplets, (non-droplet) sulfate and sea-salt) is shown in Fig. 5 as box-plot, separately for each INP/IPR sampling instrument. All INP/IPR sampling artifacts are observed for all three techniques, and their relative abundances are on comparable levels of 0–10 % for each particle type. However, in particular the Ice-CVI extracted a higher number of sea-salt particles as INP/IPR. For single measurements, the abundance of these potential sampling artifacts can reach up to 40 %.

The occurrence of sea-salt particles and of sea-salt as residual in droplets depends on the backward trajectory of the air mass. Sea-salt occurs only as INP/IPR when

ACPD
14, 23027–23073, 2014

marine air masses were sampled. In these cases, sea-salt is present in samples from all instruments.

3.2 Composition of INP/IPR at the Jungfraujoch in winter

During the field campaign 180 samples were taken, of which 7 ISI, 22 FINCH + IN-PCVI, and 14 ICE-CVI samples were analyzed with a total (non-artifact) INP/IPR particle number of approximately 2544. Due to the low number of collected INP/IPR on individual samples, the INP/IPR from all samples were added for each technique (Fig. 6) to yield better statistics. Particles were differentiated according to their size in a sub- and supermicron range.

Silicates are the main group of INP/IPR independently of sampling techniques. With all three sampling instruments, soot and sulfate particles occur mainly in the submicron range, while silicates and Ca-rich particles are predominantly found in the supermicron range. Metal oxides are present in both size ranges with a tendency to the submicron range while sea-salt particles tend to be in the supermicron range. However, if the low number of analyzed particles and the resulting statistical uncertainty are considered, the observed differences between the techniques are regarded only as a trend. In addition, the three instruments could not be operated strictly in parallel and thus, sampled different time periods. In particular, ISI samples were taken only at the end of the field campaign.

The main difference in composition trends between the three sampling methods are the high content of carbonaceous particles measured downstream of the ISI, and the high content of Pb-bearing particles obtained by Ice-CVI. The high concentration of carbonaceous particles in the ISI-samples may result from different air masses being sampled at the end of the field campaign, when ISI was operated. During this time, higher black carbon concentrations were measured than during the earlier periods (not shown). The Pb-bearing particles are discussed later in Sect. 4.4 in more detail.

If the eleven particle classes are grouped into four simplified components – particles of potential terrigenous origin (i.e., silicates and Ca-rich particles), C-dominated

ACPD
14, 23027–23073, 2014

particles (carbonaceous, soot), metal-oxides-dominated and soluble particles (sulfate, droplets, sea-salt) –the terrigenous particles are the main component with relative abundances of 40 % (ISI), 51 % (FINCH + IN-PCVI) and 55 % (Ice-CVI). The C-rich particles show a higher variation due to sampling of different air masses and range from 9 % (Ice-CVI), 13 % (FINCH + IN-PCVI) to 35 % (ISI). The soluble particles vary between 19 % (ISI and Ice-CVI) and 32 % (FINCH + IN-PCVI).

The composition of the INP/IPR-samples varies between the cloud events and between the INP/IPR sampling techniques. Figure 7 illustrates the heterogeneity of the INP/IPR composition with the example of the 2 February, where relatively stable atmospheric conditions prevailed. During this period, two samples were taken between 17:40–18:10 (Ice-CVI) and 14:50–17:11 (FINCH + IN-PCVI).

The major components show quite a consistent INP/IPR composition here, i.e., dominating silicates with a fraction of 71 % (Ice-CVI) and 65 % (FINCH + IN-PCVI) as well as the presence of organics and metal oxides. However, the relative abundance of the minor INP/IPR groups differs considerably. In particular, the group of carbonaceous particles shows a large difference between Ice-CVI (4 %) and FINCH + IN-PCVI (19 %), the same is true for the metal oxides abundance (5 % Ice-CVI, 10 % FINCH + IN-PCVI). Additionally, the ICE-CVI sample contains Pb-bearing particles (12 %) and sea-salt particles (2 %), which are absent for the FINCH + IN-PCVI sample.

3.3 Size distribution of INP/IPR components

To allow for the display of a size distribution, again we combined the detailed groups into generalized components of INP/IPR to achieve higher particle counts for each particle size interval. The resulting size distributions are shown in Fig. 8, separately for each sampling technique.

All three methods yield a maximum in the size distribution between 0.3 to 0.5 µm geometric diameter, whereas ISI shows a secondary maximum around 1 to 1.5 µm. Silicates and Ca-rich particles are predominantly found at the larger particles sizes as expected, which is particular visible for the FINCH + IN-PCVI samples. The relative

ACPD
14, 23027–23073, 2014

abundance of carbonaceous/soot is highest with the smallest particles, as is the relative abundance of the metal oxides. Again, the soluble and secondary particles do not show a particular size preference.

The maximum in the size distribution is more pronounced in the Ice-CVI samples than in FINCH + IN-PCVI and ISI samples, while ISI shows the highest relative abundance of larger particles.

3.4 Composition of total aerosol

In addition to INP/IPR composition measurements, the composition of the total aerosol was also determined for a few days. Samples of the total aerosol were taken using the Ice-CVI setup, but without the ice-selective components operating. Samples were collected at 30 January from 13:22 to 13:26 and at 16 February from 17:26 to 17:43 (UTC). While the 30 January sample was analyzed automatically, the 16 February sample was investigated manually. Therefore, droplets could be identified by morphology in the latter case. The background composition for 16 February is shown in Fig. 9 as function of particle size.

The background aerosol is dominated by sulfate and droplets (relative number abundance ~ 86–92 %) each. Silicate, soot and carbonaceous particles occur as minor components. The distribution of sulfate and droplets is inhomogeneous over the size range of the particles. Small particles (< 0.5 µm) are dominated by sulfates (approximately 75 %). The size range of 0.5 to 1 µm is dominated by the droplets. At larger particle size, both particle types occur. For the automatically analyzed sample, droplets could not be identified and were mainly classified as sulfates. Accordingly, the total aerosol of 16 February is dominated by sulfate particles. However, a larger amount of silicate particles (approximately 25 % of the particles > 1 µm) is present on this day.

ACPD
14, 23027–23073, 2014

3.5 Mixing state and Pb-bearing INP/IPR

A significant fraction of the INP/IPR consists of particles with coatings or inclusions (see groups in Fig. 6). The relative abundance of internally mixed particles for each particle type is summarized in Table 3. It is apparent that mainly silicate particles and to a lesser extent metal oxides are internally mixed. Mixing partners are mostly sulfate and carbonaceous matter, but also sea-salt, if present in the total aerosol. The other particles types are less frequently internally mixed. Regarding differences between the sampling techniques, in particular INP measured by FINCH + IN-PCVI are considerably more frequently internally mixed than IPR of the ISI and Ice-CVI. The (non-droplet) sulfates obtained as INP/IPR contain in most cases no heterogeneous inclusions. Also, most of the soot and Ca-rich particles have no coating, which is consistent for all sampling techniques. In contrast, the mixing state of carbonaceous particles was found to be highly different, rarely mixed for ISI (7 %) and frequently mixed for FINCH + IN-PCVI (64 %).

In previous IPR measurements at the JFJ station (Ebert et al., 2011; Cziczo et al., 2009b), Pb-bearing particles were found at high abundance. For comparison with the previous work (Fig. 10), we have selected the Pb-bearing particles from the total INP/IPR and determined their mixing partner. For comparability, the particles were classified in the same way as for the CLACE 5 campaign (Ebert et al., 2011). Pb-bearing particles are only found with Ice-CVI and FINCH + IN-PCVI. The Pb inclusions occur within the same main particle classes identified as INP/IPR in general, i.e., mainly silicates, Ca-rich particles, sulfates, sea-salt, and carbonaceous particles. In addition, externally mixed (homogeneous) Pb-bearing particles are present at minor abundance. While fewer externally mixed Pb-bearing particles were observed in the present field campaign (compared to Ebert et al., 2011), the abundance of the other Pb-bearing groups seems to be similar.

ACPD
14, 23027–23073, 2014

4 Discussion

4.1 Which particle classes can be regarded as INP/IPR?

Silicates have been identified as common INP/IPR in laboratory experiments as well as in field experiments (Hoose and Möhler, 2012; Murray et al., 2012). Also in our field campaign, silicates are the most abundant INP/IPR type. Ca-rich particles – e.g., carbonates like calcite – are not frequently regarded as INP, in particular as they might be subsumed with silicates as "dust" (e.g., Murray et al., 2012). However, laboratory experiments have shown that calcite can act as INP (Zimmermann et al., 2008), so also the Ca-rich particles are regarded as INP/IPR.

Metal oxides are also common ice residuals in field experiments (Chen et al., 1998; DeMott et al., 2003). Similar to our study, Fe-rich particles are the main group within the metal oxides. In addition, Al-, Ti-, Zn-, Cr-, and Ca-rich particles were found in our study and by Chen et al. (1998).

The ice nucleation ability of soot and carbonaceous particles is discussed controversially in previous literature. While an enrichment of black carbon in ice residuals has been observed in field experiments (Cozic et al., 2008) there are also other findings where organic-rich particles preferentially remain unfrozen (Cziczo et al., 2004). It has to be mentioned, however, that carbon-rich particles are sometimes named ambiguously depending on the technique used for analysis (see also Murray et al., 2012; Petzold et al., 2013). Thus, uncertainties may arise from ambiguous identification of carbonaceous particles. Laboratory experiments show that the ice forming activity of soot is influenced by size, surface area and the concentration of the surface chemical groups that can form hydrogen bonds with water molecules (Koehler et al., 2009; Gorbunov et al., 2001). According to the latter, the ice forming activity of soot is close to that of metal oxides. In summary, we conclude that the soot and the carbonaceous particles observed in our samples were active as INP.

Based on field experiments and laboratory studies, Pb-bearing particles are in general regarded as good ice nuclei (for a detailed discussion refer to Cziczo et al., 2009b).

ACPD
14, 23027–23073, 2014

In the present study, lead is found mainly in two states, as homogeneous Pb-rich particles and as Pb-rich inclusions in other INP/IPR. Some fraction of the large homogeneous Pb-rich particles might be regarded as artifact, as the Ice-CVI impaction plates consist of a Pb-bearing aluminum alloy. SEM inspection of the impaction plates revealed the presence of lead particles, which might be resuspended on ice particle impact. The small lead inclusions in other INP/IPR are not regarded as potential artifact. However, only a small fraction of the large homogeneous Pb-rich particles found in the ICE-CVI may be an artifact, as similar particles were also observed in the FINCH + INPCVI samples, where no Pb-containing aluminum alloy was used. As an exact estimate of the lead artifact abundance cannot be provided, all homogeneous Pb-rich particles are considered as INP/IPR. This assumption also applies to previous studies at the JFJ station (Ebert et al., 2011; Cziczo et al., 2009b).

The ice nucleation ability of secondary aerosol particles is discussed controversially in the literature. As in the case of soot and carbonaceous matter, secondary aerosol particles are found in field measurements of INP (Abbatt et al., 2006; Prenni et al., 2009b) and in laboratory experiments under cirrus cloud conditions (Hoose and Möhler, 2012). In contrast, Cziczo et al. (2004) report that organic-rich particles (internally mixed particles of sulfates and organic spezies) preferentially remain unfrozen. Based on our data, whereby secondary material is present in many INP/IPR samples and does not have a high abundance in the total aerosol, we consider these particles as INP/IPR.

Sea-salt as INP/IPR was described by Cziczo and Froyd (2014) and Targino et al. (2006). While crystalline salts were found to be able to act as INP under upper-tropospheric conditions (Zuberi et al., 2001), there has been a lack in clarifying the process by which a hygroscopic and soluble material should act as IN. However, recently Wise et al. (2012) explained this behavior by fractional crystallization of the solute component under decreasing temperatures. Based on these findings, we consider sea-salt as INP/IPR.

ACPD
14, 23027–23073, 2014

The ice nucleation ability of sulfate particles is also discussed controversially in the literature. Sulfates may act as INP in cirrus clouds in the upper troposphere and lower stratosphere, both in immersion and deposition modes (Abbatt et al., 2006, and references therein; Hoose and Möhler, 2012). Sulfates acting as INP are found in field experiments when cold temperatures dominate (Twohy and Poellot, 2005), but usually not in the warmer mixed phase clouds as encountered during our field experiment. If we consider the high relative abundance of sulfates in the total aerosol, we cannot exclude the possibility that sulfates are simply an artifact of the INP/IPR discrimination techniques not having perfect (i.e., 100 %) discrimination efficiency. Thus, we consider sulfate particles not to be INP/IPR. Nevertheless, we provide data on their abundance. Similar considerations apply to the observed droplets.

As explained in the methods section, contamination artifact particles were removed from the further analysis.

Concluding, we regard silicates and Ca-rich particles, metal oxides, Pb-bearing particles, soot, carbonaceous particles, secondary particles and sea-salt as "real" INP/IPR, while sulfate and droplets are judged as sampling artifacts.

4.2 Relative ice nucleation ability of the different particle classes

By comparing the relative abundance of the different particle classes within the INP/IPR samples and the total aerosol samples, enrichment factors and the relative ice nucleation efficiency at the given conditions could be calculated. However, this approach is hampered due to the very low particle numbers of the INP/IPR samples and the low abundance of non-sulfate/non-droplet particles in the total aerosol. Nevertheless, some qualitative statements on the relative ice nucleation efficiency can be made.

While the total aerosol is dominated by sulfate and droplets (Fig. 9), these two compounds were observed at a low abundance in the INP/IPR samples, independently of the sampling techniques (Fig. 6). Thus, sulfate and droplets can only have a very low INP efficiency, or could even be considered as an sampling artifact (see previous section).

ACPD
14, 23027–23073, 2014

In contrast, the relative abundance of silicates is considerable higher in the INP/IPR fraction than in the total aerosol, pointing to its high IN efficiency, which is consistent with earlier results from the JFJ station and from laboratory experiments (Ebert et al., 2011; Hoose and Möhler, 2012). Recently, feldspar minerals and in particular K-rich feldspars were discussed as efficient INP (Atkinson et al., 2013; Yakobi-Hancock et al., 2013). Despite the fact that we did not determine the mineralogical phase of the silicate particles, we can show by SEM-EDX that they are not rich in potassium. Thus, it is concluded that K-rich feldspar particles do not play a role as INP/IPR at Jungfraujoch in winter. The Ca-rich particles – probably also of terrigenous origin – were not detected in the total aerosol, which may result from statistical limitations or from a highly variable composition. In the supermicron fraction of the INP/IPR samples, however, they appear with a number abundance ratio of 1 : 10 to 1 : 3 relative to silicates (depending on method and sample), which is in the range reported for natural mineral dust (Kandler et al., 2007, 2009; Coz et al., 2009). Thus, they can be considered as similarly effective as silicates, which is consistent with laboratory experiments for calcite (Zimmermann et al., 2008).

Carbonaceous material is also considerably enriched in the INP/IPR samples in comparison to the total aerosol. Based on their unspecific morphology and the absence of tracer elements (e.g., N, P, K) these particles are not regarded as primary biological particles. It is assumed that the carbonaceous material consists of organic compounds which condensed from the gas phase.

Soot is less enriched than silicates and carbonaceous material in the INP/IPR samples, so it seems to be less efficient as INP. Sea-salt appears as INP/IPR only during advection of marine air masses.

With regard to the mixing state, particularly the difference between silicates and Ca-rich particles is notable. While silicates are usually internally mixed, the Ca-rich particles do not have a detectable coating. This may indicate that for a silicate particle a coating is less effective in reducing its IN ability than for a Ca-rich particle, pointing to a more pronounced processing (e.g., destruction of the surface structure) of the

ACPD
14, 23027–23073, 2014

former. However, there is lack of agreement on the influence of coatings on the ice nucleation ability of silicates in literature. In field experiments, coatings on silicates and metal oxides are commonly observed (Targino et al., 2006; Chen et al., 1998; Prenni et al., 2009a). In laboratory experiments, conflicting results are obtained. While Cziczo et al. (2009a) as well as Hoose and Möhler (2012) found a deactivation of the ice nuclei due to coatings, Sullivan et al. (2010) reported that coatings may have no effect on the ice nucleation ability. Instead, Archuleta et al. (2005) and Zuberi et al. (2002) discuss mineral dust as efficient nucleus for ice in NH_4SO_4–H_2O aerosols and demonstrated that mineral particles coated with sulfate increase the freezing temperature up to 10 K compared to pure sulfate solutions. Richardson et al. (2007) reported that soluble coatings favor condensation-freezing nucleation and inhibit nucleation by vapor deposition. But they also mention, that coatings itself may act either to increase or decrease ice nucleation efficiency independent of the nucleation mechanism.

In summary, the range of the fraction of mixed particles in the present field experiment is similar to previous literature. Chen et al. (1998) reported a fraction up to 25 % of INP which were mixtures of sulfates and elements indicative of insoluble particles. The same relative abundance of mixtures of metal oxides/dust with either carbonaceous components or salts/sulfates was reported by Prenni et al. (2009a). For the JFJ station, a slightly lower fraction of internally mixed particles was found during the CLACE 5/6 campaigns: 9–15 % by Ebert et al. (2011) and up to 15 % by Kamphus et al. (2010).

4.3 Comparison between FINCH + IN-PCVI, Ice-CVI and ISI

A reasonable agreement between the different sampling techniques is obtained for the major particle groups observed among the INP/IPR. However, the variation in INP/IPR composition due to meteorological conditions in connection with the non-parallel sampling introduces a systematic error. The non-parallel sampling could not be avoided during the present field campaign, as the sampling techniques were not yet in a state allowing for synchronized operation. Consequently, INP/IPR composition snapshots from different time periods needed to be integrated for comparison.

ACPD
14, 23027–23073, 2014

In contrast, extreme differences in the mixing state were observed depending on sampling technique (Table 3). While the difference in relative abundance of internally mixed particles between Ice-CVI and ISI might be explained by the considerably different sampling times, this is not the case for FINCH + IN-PCVI. In particular, it is surprising, that FINCH + IN-PCVI measures in general higher abundances of internally mixed particles in comparison to the other two methods, as from the ice-nucleating mechanisms (Table 1) – i.e. the lack of contact freezing in FINCH + IN-PCVI – the opposite effect would be expected. This demonstrates that the influence of the systematic differences of the INP/IPR-separating techniques on the composition of the INP/IPR is not yet fully understood.

4.4 Comparison with other field experiments

If all INP/IPR particles of the three sampling methods are summed up, the following averaged INP/IPR composition of the whole field campaign is obtained: 52 % terrigenous particles (38 % silicates, 9 % metal oxides, 5 % Ca-rich particles), 14 % C-rich (12 % carbonaceous particles, 2 % soot), 1 % secondary particles, 11 % sulfate, 11 % droplets, 4 % sea-salt, 5 % Pb-bearing particles, and 2 % other particles.

A comparable INP composition was reported by Prenni et al. (2009a) for the field campaign M-PACE with 64 % terrigenous particles (39 % metal oxides/dust + 25 % mixtures of metal oxides/dust with either carbonaceous components or salts/sulfate), and 35 % carbonaceous particles. Also, Targino et al. (2006) reported an IN composition of 57.5 % alumosilicates, Fe-rich, and Si-rich, 23.3 % low atomic number (presumably organic), and 6.7 % sea-salt. They observed sulfur coatings for all groups indicating ageing and in-cloud processing. For the CLACE 6 field experiment Kamphus et al. (2010) found an IPR composition of 60 % mineral dust and 25 % sulfate/organic. The remaining 15 % were mixed particles and biomass burning particles. In the same field experiment, Pb-bearing particles, complex internal mixtures with silicates and metal oxides as major component as well as internal mixtures of secondary aerosol with carbonaceous material were found to be strongly enriched in IPR relative to the interstitial

ACPD
14, 23027–23073, 2014

aerosol and, thus, regarded as effective INP (Ebert et al., 2011). An overview of IPR compositions found during 13 field campaigns of cirrus clouds is given by Cziczo and Froyd (2014). The main groups were mineral dust, metals, BC/soot, sea-salt, sulfate, and biomass burning.

In summary, it can be concluded that the mean composition of the INP/IPR encountered at the JFJ station during our field campaign fits well into the range observed in previous experiments.

Similar to the ice nucleation efficiency (as determined from the observed enrichment of particle groups within INP/IPR relative to the aerosol) reported in the present study (see above), Chen et al. (1998) and DeMott et al. (2003) found an enrichment of metallic, crustal, and carbonaceous fraction.

The observed high variability in INP/IPR composition at the JFJ station found in the present study is consistent with other field experiments. For example, Targino et al. (2006) reported a strong dependency of INP composition on air mass history. Continentally-influenced air masses contained mainly mineral dust residuals, while clean air masses were dominated by low-Z (presumably secondary aerosol) and sea-salt particles. Sulfates are mainly found in field experiments when cold temperatures dominate (Cziczo and Froyd, 2014; Twohy and Poellot, 2005). A high variability of INP composition as function of air mass history is also reported by DeMott et al. (2003).

A relative high abundance of Pb-bearing particles, in particular internally mixed ones, seems to be characteristic for IPR at the JFJ station. They were identified by earlier measurements (Ebert et al., 2011; Cziczo et al., 2009b) and during the present filed campaign. However, the fraction of Pb-bearing particles in the whole INUIT campaign is 1 % for FINCH + IN-PCVI, and 10 % for Ice-CVI. In contrast, a higher fraction of up to 20 % was found during CLACE 5. As helicopter flights – where Pb-rich particles might be emitted due to leaded fuel usage – observed around the Jungfraujoch station were more frequent during CLACE 5 than during the present field campaign, this would indicate a considerable contribution of local emission to the IN formation at JFJ station.

ACPD
14, 23027–23073, 2014

4.5 Comparison between scanning electron microscopy analysis and laser ablation mass spectrometry

The results of energy-dispersive X-ray microanalysis in the scanning electron microscope (SEM-EDX) of the collected INP/IPR particles can be compared to the findings of online laser ablation mass spectrometry (LA-MS). Unfortunately, both techniques could not be run in parallel. Due to the low INP/IPR concentrations, it was necessary to sum up all available data, which may lead to systematic errors due to a high variation in the chemical composition of the IPR fraction as function of changing air masses and meteorological conditions. Furthermore, for a comparison between SEM-EDX and LA-MS a more general particle classification scheme, combining the detailed SEM-EDX groups, was necessary.

The average particle group number abundance, derived by SEM-EDX – separately for all IPR from ISI and Ice-CVI – is compared in Fig. 11 to the results of the laser ablation mass spectrometer ALABAMA (Schmidt et al., 2014). The most obvious difference between the two approaches is the presence of 10–18 % of secondary particles (mostly mixtures of sulfates/nitrates and/or organics), pure sulfates and droplets (residuals of volatile species like nitrates and organics) in SEM-EDX. These groups are completely absent in LA-MS. This difference may be explained by the fact that anions were not measured by LA-MS during the present campaign.

For the other groups, a fair agreement of the results is obtained. First, the sum of sea-salt, carbonaceous material, soot and mineral dust (orange and green groups) contributes 70–90 % to the IPR. Second, metal oxides (based on SEM-EDX mainly iron oxides) occur at an abundance of 5–10 %. Third, Ice-CVI samples contain Pb-rich particles (5–10 %), while these particles are absent in ISI.

However, pronounced discrepancies exist between SEM-EDX and LA-MS data, in particular for Ice-CVI. For this sampling technique, a lower abundance of carbonaceous matter is found by SEM-EDX, and a higher abundance of silicates. This quantitative comparison of compositional data from both analysis techniques is hampered

ACPD
14, 23027–23073, 2014

by the different approach in particle characterization. The particle classification with SEM-EDX relies on the characteristic X-ray signals, which can be used to quantify the chemical composition of a particle. Our classification scheme uses only the major elements detected inside a particle to assign it to an according group. Minor elements are mostly neglected in particle classification, trace elements cannot be measured at all. In contrast, single particle LA-MS relies on ionized compounds, so ionization efficiency plays a major role. Thus, strong signals often originate from the atoms or molecules, which can be best ionized in LA-MS, but are not necessarily a major component of the particles. While LA-MS works usually well for externally mixed particles, problems can arise for the classification of internally mixed particles. In our particular case, it cannot be excluded that, for example, a silicate particle with a thin organic coating is classified as silicate in SEM-EDX (based on Si as major element), but as carbonaceous particle in LA-MS (based on a strong signal of ionized carbonaceous matter). This example clearly demonstrates the need for further systematical comparison between these two analytical techniques.

5 Summary and conclusions

For the first time, the chemical composition of individual INP/IPR collected by three techniques – ISI, FINCH + IN-PCVI and Ice-CVI – was analyzed in a field experiment. In winter, the INP/IPR composition at the JFJ station is composed of five main groups: the dominating potential terrigenous silicates/Ca-rich particles, carbonaceous particles, the metal oxides/hydroxides like Fe-, Ti, or Al-oxides/hydroxides, soot, and probably soluble particles like sea-salt. Identified sulfates and droplets were not considered as INP/IPR. Lead inclusions occur in several INP/IPR, while large homogeneous Pb-rich particles must be considered partially as artifacts. As the composition is in principle similar to earlier field experiments, and the methods agree roughly regarding major and minor components, we consider this experiment as a successful step in

ACPD
14, 23027–23073, 2014

providing INP/IPR chemical composition by different techniques. This is supported by the agreement regarding in the maximum of INP/IPR size distributions.

For all three INP/IPR separation techniques, different contamination artifacts and potential sampling artifacts were identified. These artifacts are easily detectable by the chemical and morphological analysis. In contrast, counting or size distribution techniques would consider these contamination and sampling artifacts as real INP/IPR and, consequently, overestimate the INP/IPR concentration. Thus, the present work provides information suitable for correction of counting techniques, for the contamination artifacts as well as for sampling artifacts. While for the former correction is necessary, interpretation of the latter might change with advancing knowledge regarding the INP/IPR abilities of soluble compounds.

Deeper data investigation reveals that beyond the agreement in maximum of the INP/IPR size distribution there are considerable differences between the instruments pointing to different efficiencies in INP activation and IPR separation. This is particularly obvious when we consider the large difference in internally-mixed particle abundance. While a part of these discrepancies might be explained by atmospheric variability in connection with non-parallel sampling (an issue, which is expected to be overcome in future experiments by increased stability in instrument operation), they also indicate lack in understanding regarding the chemical selectivity of the different INP/IPR-discriminating techniques.

Acknowledgements. We gratefully acknowledge financial support by the Deutsche Forschungsgemeinschaft within the research group "Ice Nuclei Research Unit INUIT" (FOR 1525). We thank Emanuel Hammer and Gary Lloyd for providing the liquid water content data and MeteoSwiss/EMPA for the meteorological data.

We also thank Stephan Günnel (Institut für Troposphärenforschung, Leipzig, Germany) for his help in setting up the Ice-CVI on the platform of the Sphinx Laboratory at the Jungfraujoch Research Station.

We also thank the International Foundation High Altitude Research Stations Jungfraujoch and Gornergrat (HFSJG) for the opportunity to perform experiments on the Jungfraujoch.

ACPD
14, 23027–23073, 2014

References

Abbatt, J. P. D., Benz, S., Cziczo, D. J., Kanji, Z., Lohmann, U., and Möhler, O.: Solid ammonium sulfate aerosols as ice nuclei: a pathway for cirrus cloud formation, Science, 313, 1770–1773, doi:10.1126/science.1129726, 2006.

Archuleta, C. M., DeMott, P. J., and Kreidenweis, S. M.: Ice nucleation by surrogates for atmospheric mineral dust and mineral dust/sulfate particles at cirrus temperatures, Atmos. Chem. Phys., 5, 2617–2634, doi:10.5194/acp-5-2617-2005, 2005.

Atkinson, J. D., Murray, B. J., Woodhouse, M. T., Whale, T. F., Baustian, K. J., Carslaw, K. S., Dobbie, S., O'Sullivan, D., and Malkin, T. L.: The importance of feldspar for ice nucleation by mineral dust in mixed-phase clouds, Nature, 498, 355–358, doi:10.1038/nature12278, 2013.

Brands, M., Kamphus, M., Böttger, T., Schneider, J., Drewnick, F., Roth, A., Curtius, J., Voigt, C., Borbon, A., Beekmann, M., Bourdon, A., Perrin, T., and Borrmann, S.: Characterization of a newly developed Aircraft-Based Laser Ablation Aerosol Mass Spectrometer (ALABAMA) and first field deployment in urban pollution plumes over Paris during MEGAPOLI 2009, Aerosol Sci. Tech., 45, 46–64, doi:10.1080/02786826.2010.517813, 2011.

Bundke, U., Nillius, B., Jaenicke, R., Wetter, T., Klein, H., and Bingemer, H.: The Fast Ice Nucleus Chamber FINCH, Atmos. Res., 90, 180–186, doi:10.1016/j.atmosres.2008.02.008, 2008.

Bundke, U., Reimann, B., Nillius, B., Jaenicke, R., and Bingemer, H.: Development of a Bioaerosol single particle detector (BIO IN) for the Fast Ice Nucleus CHamber FINCH, Atmos. Meas. Tech., 3, 263–271, doi:10.5194/amt-3-263-2010, 2010.

Chen, Y., Kreidenweis, S. M., McInnes, L. M., Rogers, D. C., and DeMott, P. J.: Single particle analyses of ice nucleating aerosols in the upper troposphere and lower stratosphere, Geophys. Res. Lett., 25, 1391–1394, 1998.

Collaud Coen, M., Weingartner, E., Furger, M., Nyeki, S., Prévôt, A. S. H., Steinbacher, M., and Baltensperger, U.: Aerosol climatology and planetary boundary influence at the Jungfraujoch analyzed by synoptic weather types, Atmos. Chem. Phys., 11, 5931–5944, doi:10.5194/acp-11-5931-2011, 2011.

Coz, E., Gómez-Moreno, F. J., Pujadas, M., Casuccio, G. S., Lersch, T. L., and Artíñano, B.: Individual particle characteristics of North African dust under different long-range transport scenarios, Atmos. Environ., 43, 1850–1863, 2009.

ACPD
14, 23027–23073, 2014

Cozic, J., Mertes, S., Verheggen, B., Cziczo, D. J., Gallavardin, S. J., Walter, S., Baltensperger, U., and Weingartner, E.: Black carbon enrichment in atmospheric ice particle residuals observed in lower tropospheric mixed phase clouds, J. Geophys. Res., 113, D15209, doi:10.1029/2007jd009266, 2008.

Cziczo, D. J. and Froyd, K. D.: Sampling the composition of cirrus ice residuals, Atmos. Res., 142, 15–31, doi:10.1016/j.atmosres.2013.06.012, 2014.

Cziczo, D. J., DeMott, P. J., Brooks, S. D., Prenni, A. J., Thomson, D. S., Baumgardner, D., Wilson, J. C., Kreidenweis, S. M., and Murphy, D. M.: Observations of organic species and atmospheric ice formation, Geophys. Res. Lett., 31, L12116, doi:10.1029/2004gl019822, 2004.

Cziczo, D. J., Froyd, K. D., Gallavardin, S. J., Möhler, O., Benz, S., Saathoff, H., and Murphy, D. M.: Deactivation of ice nuclei due to atmospherically relevant surface coatings, Environ. Res. Lett., 4, 044013, doi:10.1088/1748-9326/4/4/044013, 2009a.

Cziczo, D. J., Stetzer, O., Worringen, A., Ebert, M., Weinbruch, S., Kamphus, M., Gallavardin, S. J., Curtius, J., Borrmann, S., Froyd, K. D., Mertes, S., Möhler, O., and Lohmann, U.: Inadvertent climate modification due to anthropogenic lead, Nat. Geosci., 2, 333–336, doi:10.1038/ngeo499, 2009b.

DeMott, P. J., Cziczo, D. J., Prenni, A. J., Murphy, D. M., Kreidenweis, S. M., Thomson, D. S., Borys, R., and Rogers, D. C.: Measurements of the concentration and composition of nuclei for cirrus formation, P. Natl. Acad. Sci. USA, 100, 14655–14660, doi:10.1073/pnas.2532677100, 2003.

Ebert, M., Worringen, A., Benker, N., Mertes, S., Weingartner, E., and Weinbruch, S.: Chemical composition and mixing-state of ice residuals sampled within mixed phase clouds, Atmos. Chem. Phys., 11, 2805–2816, doi:10.5194/acp-11-2805-2011, 2011.

Flato, G., Marotzke, J., Abiodun, B., Braconnot, P., Chou, S. C., Collins, W., Cox, P., Driouech, F., Emori, S., Eyring, V., Forest, C., Gleckler, P., Guilyardi, E., Jakob, C., Kattsov, V., Reason, C., and Rummukainen, M.: Evaluation of Climate Models, in: Climate Change 2013: The Physical Science Basis. Contribution of Working Group I to the Fifth Assessment Report of the Intergovernmental Panel on Climate Change, edited by: Stocker, T. F., Qin, D., Plattner, G.-K., Tignor, M., Allen, S. K., Boschung, J., Nauels, A., Xia, Y., Bex, V., and Midgley, P. M., Cambridge University Press, Cambridge, United Kingdom and New York, NY, USA, 741–866, 2013.

Gorbunov, B., Baklanov, A., Kakutkina, N., Windsor, H. L., and Toumi, R.: Ice nucleation on soot particles, J. Aerosol Sci., 32, 199–215, doi:10.1016/S0021-8502(00)00077-X, 2001.

ACPD
14, 23027–23073, 2014

Hoose, C. and Möhler, O.: Heterogeneous ice nucleation on atmospheric aerosols: a review of results from laboratory experiments, Atmos. Chem. Phys., 12, 9817–9854, doi:10.5194/acp-12-9817-2012, 2012.

Hu, Y.-X., Yang, P., Lin, B., Gibson, G., and Hostetler, C.: Discriminating between spherical and non-spherical scatterers with lidar using circular polarization: a theoretical study, J. Quant. Spectrosc. Ra., 79–80, 757–764, doi:10.1016/S0022-4073(02)00320-5, 2003.

HYSPLIT (HYbrid Single-Particle Lagrangian Integrated Trajectory) Model access via NOAA ARL READY Website, available at: http://www.arl.noaa.gov/HYSPLIT.php (last access: 20 March 2014), 2013.

Kamphus, M., Ettner-Mahl, M., Klimach, T., Drewnick, F., Keller, L., Cziczo, D. J., Mertes, S., Borrmann, S., and Curtius, J.: Chemical composition of ambient aerosol, ice residues and cloud droplet residues in mixed-phase clouds: single particle analysis during the Cloud and Aerosol Characterization Experiment (CLACE 6), Atmos. Chem. Phys., 10, 8077–8095, doi:10.5194/acp-10-8077-2010, 2010.

Kandler, K., Benker, N., Bundke, U., Cuevas, E., Ebert, M., Knippertz, P., Rodríguez, S., Schütz, L., and Weinbruch, S.: Chemical composition and complex refractive index of Saharan Mineral Dust at Izaña, Tenerife (Spain) derived by electron microscopy, Atmos. Environ., 41, 8058–8074, doi:10.1016/j.atmosenv.2007.06.047, 2007.

Kandler, K., Schütz, L., Deutscher, C., Hofmann, H., Jäckel, S., Knippertz, P., Lieke, K., Massling, A., Schladitz, A., Weinzierl, B., Zorn, S., Ebert, M., Jaenicke, R., Petzold, A., and Weinbruch, S.: Size distribution, mass concentration, chemical and mineralogical composition, and derived optical parameters of the boundary layer aerosol at Tinfou, Morocco, during SAMUM 2006, Tellus B, 61, 32–50, doi:10.1111/j.1600-0889.2008.00385.x, 2009.

Klein, H., Haunold, W., Bundke, U., Nillius, B., Wetter, T., Schallenberg, S., and Bingemer, H.: A new method for sampling of atmospheric ice nuclei with subsequent analysis in a static diffusion chamber, Atmos. Res., 96, 218–224, doi:10.1016/j.atmosres.2009.08.002, 2010.

Koehler, K. A., DeMott, P. J., Kreidenweis, S. M., Popovicheva, O. B., Petters, M. D., Carrico, C. M., Kireeva, E. D., Khokhlova, T. D., and Shonija, N. K.: Cloud condensation nuclei and ice nucleation activity of hydrophobic and hydrophilic soot particles, Phys. Chem. Chem. Phys., 11, 7906–7920, doi:10.1039/b905334b, 2009.

Kupiszewski, P., Weingartner, E., Vochezer, P., Schnaiter, M., Bigi, A., Gysel, M., Baltensperger, U., and Wehrle, G.: Ice Selective Inlet: setup and first applications, Atmos. Meas. Tech. Discuss., in preparation, 2014.

ACPD
14, 23027–23073, 2014

Lohmann, U. and Feichter, J.: Global indirect aerosol effects: a review, Atmos. Chem. Phys., 5, 715–737, doi:10.5194/acp-5-715-2005, 2005.

Mertes, S., Galgon, D., Schwirn, K., Nowak, A., Lehmann, K., Massling, A., Wiedensohler, A., and Wieprecht, W.: Evolution of particle concentration and size distribution observed upwind, inside and downwind hill cap clouds at connected flow conditions during FEBUKO, Atmos. Environ., 39, 4233–4245, 2005a.

Mertes, S., Lehmann, K., Nowak, A., Massling, A., and Wiedensohler, A.: Link between aerosol hygroscopic growth and droplet activation observed for hill-capped clouds at connected flow conditions during FEBUKO, Atmos. Environ., 39, 4247–4256, 2005b.

Mertes, S., Verheggen, B., Walter, S., Connolly, P., Ebert, M., Schneider, J., Bower, K. N., Cozic, J., Weinbruch, S., Baltensperger, U., and Weingartner, E.: Counterflow virtual impactor based collection of small ice particles in mixed-phase clouds for the physico-chemical characterization of tropospheric ice nuclei: sampler description and first case study, Aerosol Sci. Tech., 41, 848–864, doi:10.1080/02786820701501881, 2007.

Murray, B. J., O'Sullivan, D., Atkinson, J. D., and Webb, M. E.: Ice nucleation by particles immersed in supercooled cloud droplets, Chem. Soc. Rev., 41, 6519–6554, doi:10.1039/c2cs35200a, 2012.

Petzold, A., Ogren, J. A., Fiebig, M., Laj, P., Li, S.-M., Baltensperger, U., Holzer-Popp, T., Kinne, S., Pappalardo, G., Sugimoto, N., Wehrli, C., Wiedensohler, A., and Zhang, X.-Y.: Recommendations for reporting "black carbon" measurements, Atmos. Chem. Phys., 13, 8365–8379, doi:10.5194/acp-13-8365-2013, 2013.

Prenni, A. J., Demott, P. J., Rogers, D. C., Kreidenweis, S. M., McFarquhar, G. M., Zhang, G., and Poellot, M. R.: Ice nuclei characteristics from M-PACE and their relation to ice formation in clouds, Tellus B, 61, 436–448, doi:10.1111/j.1600-0889.2009.00415.x, 2009a.

Prenni, A. J., Petters, M. D., Faulhaber, A., Carrico, C. M., Ziemann, P. J., Kreidenweis, S. M., and DeMott, P. J.: Heterogeneous ice nucleation measurements of secondary organic aerosol generated from ozonolysis of alkenes, Geophys. Res. Lett., 36, L06808, doi:10.1029/2008gl036957, 2009b.

Richardson, M. S., DeMott, P. J., Kreidenweis, S. M., Cziczo, D. J., Dunlea, E. J., Jimenez, J. L., Thomson, D. S., Ashbaugh, L. L., Borys, R. D., Westphal, D. L., Casuccio, G. S., and Lersch, T. L.: Measurements of heterogeneous ice nuclei in the western United States in springtime and their relation to aerosol characteristics, J. Geophys. Res., 112, D02209, doi:10.1029/2006jd007500, 2007.

ACPD
14, 23027–23073, 2014

Schenk, L. A. E. A.: Counterflow virtual impactor technique for the characterization of ice nuclei detected by an ice nucleus counter, in preparation, Atmos. Meas. Tech. Discuss., 2014.
Scheuvens, D., Kandler, K., Küpper, M., Lieke, K., Zorn, S., Ebert, M., Schütz, L., and Weinbruch, S.: Indiviual-particle analysis of airborne dust samples collected over Morocco in 2006 during SAMUM 1, Tellus B, 63, 512–530, doi:10.1111/j.1600-0889.2011.00554.x, 2011.
Schmidt, S., Schneider, J., Klimach, T., Mertes, S., Schenk, L., Kästner, U., Stratmann, F., Curtius, J., Kupiszewski, P., Weingartner, E., Hammer, E., Vochez, P., Schnaiter, M., Ebert, M., Worringen, A., Kandler, K., Weinbruch, S., and Borrmann, S.: In-situ single particle composition analysis of ice residuals in mixed-phase clouds during INUIT-JFJ 2013, Atmos. Chem. Phys. Discuss., in preparation, INUIT special issue, 2014.
Sullivan, R. C., Miñambres, L., DeMott, P. J., Prenni, A. J., Carrico, C. M., Levin, E. J. T., and Kreidenweis, S. M.: Chemical processing does not always impair heterogeneous ice nucleation of mineral dust particles, Geophys. Res. Lett., 37, L24805, doi:10.1029/2010gl045540, 2010.
Targino, A. C., Krejci, R., Noone, K. J., and Glantz, P.: Single particle analysis of ice crystal residuals observed in orographic wave clouds over Scandinavia during INTACC experiment, Atmos. Chem. Phys., 6, 1977–1990, doi:10.5194/acp-6-1977-2006, 2006.
Twohy, C. H. and Poellot, M. R.: Chemical characteristics of ice residual nuclei in anvil cirrus clouds: evidence for homogeneous and heterogeneous ice formation, Atmos. Chem. Phys., 5, 2289–2297, doi:10.5194/acp-5-2289-2005, 2005.
WDCA: The World Data Centre for Aerosols, available at: http://www.gaw-wdca.org (last access: 19 March 2014), 2014.
Weingartner, E., Nyeki, S., and Baltensperger, U.: Seasonal and diurnal variation of aerosol size distributions ($10 < D < 750$ nm) at a high-alpine site (Jungfraujoch 3580 m asl), J. Geophys. Res., 104, 26809–26820, doi:10.1029/1999JD900170, 1999.
Wex, H., DeMott, P. J., Tobo, Y., Hartmann, S., Rösch, M., Clauss, T., Tomsche, L., Niedermeier, D., and Stratmann, F.: Kaolinite particles as ice nuclei: learning from the use of different kaolinite samples and different coatings, Atmos. Chem. Phys., 14, 5529–5546, doi:10.5194/acp-14-5529-2014, 2014.
Wise, M. E., Baustian, K. J., Koop, T., Freedman, M. A., Jensen, E. J., and Tolbert, M. A.: Depositional ice nucleation onto crystalline hydrated NaCl particles: a new mechanism for ice formation in the troposphere, Atmos. Chem. Phys., 12, 1121–1134, doi:10.5194/acp-12-1121-2012, 2012.

ACPD
14, 23027–23073, 2014

Yakobi-Hancock, J. D., Ladino, L. A., and Abbatt, J. P. D.: Feldspar minerals as efficient deposition ice nuclei, Atmos. Chem. Phys., 13, 11175–11185, doi:10.5194/acp-13-11175-2013, 2013.

Zimmermann, F., Weinbruch, S., Schütz, L., Hofmann, H., Ebert, M., Kandler, K., and Worringen, A.: Ice nucleation properties of the most abundant mineral dust phases, J. Geophys. Res., 113, D23204, doi:10.1029/2008JD010655, 2008.

Zuberi, B., Bertram, A. K., Koop, T., Molina, L. T., and Molina, M. J.: Heterogeneous freezing of aqueous particles induced by crystallized $(NH_4)_2SO_4$, ice, and letovicite, Phys. Chem. A, 105, 6458–6464, doi:10.1021/jp010094e, 2001.

Zuberi, B., Bertram, A. K., Cassa, C. A., Molina, L. T., and Molina, M. J.: Heterogeneous nucleation of ice in $(NH_4)_2SO_4$–H_2O particles with mineral dust immersions, Geophys. Res. Lett., 29, 142-141–142-144, doi:10.1029/2001gl014289, 2002.

ACPD
14, 23027–23073, 2014

Table 1. Techniques and operation principles used for ice-nucleating particle (INP) and ice particle residual (IPR) differentiation.

INP/IPR-separating technique	Principle of operation	Mode of operation	Ice nucleation location	Separated particle type	Freezing mechanisms	Size fraction of sampled ice particles
Fast Ice Nucleus Counter (FINCH) + Ice Nuclei pumped Counter-flow Virtual Impactor (IN-PCVI)	activation of INP under suitable thermodynamic conditions, separation of INP by inertia	in-cloud and out of cloud, discontinuous	instrument	INP	deposition, condensation, immersion	$d > 2\,\mu m$
Ice-Counterflow Virtual Impactor (Ice-CVI)	removal of supercooled droplets, transmission of ice particles	in-cloud, continuous	atmosphere	IPR	deposition, condensation, immersion, contact	$5 < d < 20\,\mu m$
Ice Selective Inlet (ISI)	use of Bergeron–Findeisen process to evaporate supercooled droplets, transmission of ice particles	in-cloud, continuous	atmosphere	IPR	deposition, condensation, immersion, contact	$4.9\,\mu m < d < 20\,\mu m$

ACPD
14, 23027–23073, 2014

Table 2. Classification criteria for particle classes and particle groups. Common features for certain particle types not used for classification are given in parentheses.

Class	Group	Chemistry	Morphologyy	Mixing state	Beam stability
Carbonaceous	carbonaceous carbonaceous + inclusion	C C	non-soot non-soot	no inclusion inclusion	
Secondary	secondary	C, O, S			
Sulfate	sulfate sulfate + inclusion	S, O, (Na, K) S, O, (Na, K)		no residual residual	unstable unstable
Soot	soot soot mixture	C C	soot-like soot-like	no coating coating	
Sea-salt	sea-salt sea-salt + inclusion	Na, Cl, (K, Mg) Na, Cl, (K, Mg)		no inclusion inclusion	
Ca-rich	Ca-rich Ca-rich + inclusion	Ca, O, (Mg, S, C) Ca, O, (Mg, S, C)		no inclusion inclusion	
Metal oxide	metal oxide metal oxide + coating	Fe, Al, Ti, (Mn) Fe, Al, Ti, (Mn)		no coating coating	
Silicate	silicate silicate mixture	Si, Al, (K, Ca, Mg, Fe, Ti) Si, Al, (K, Ca, Mg, Fe, Ti)		no coating coating or agglomerates	
Pb-bearing	Pb-bearing	Pb present			
Droplet	droplet		particle centered in ring of smaller particles		
Other	other				

ACPD
14, 23027–23073, 2014

Table 3. Relative abundance of mixed/coated particles in each particle class for each technique.

Particle group	FINCH + IN-PCVI	Ice-CVI	ISI
Silicate	61 %	37 %	59 %
Ca-rich	8 %	9 %	9 %
Metal oxide	67 %	40 %	4 %
Carbonaceous	64 %	29 %	7 %
Soot	14 %	6 %	13 %
Sea-salt	54 %	9 %	10 %
Sulfate	2 %	4 %	0 %

ACPD
14, 23027–23073, 2014

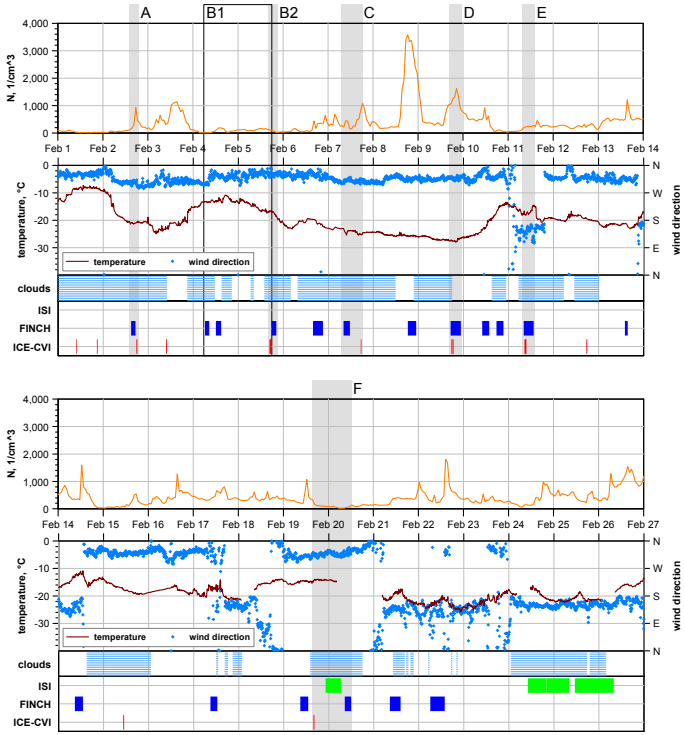

Figure 1. Atmospheric conditions and INP/IPR sampling periods in February 2013. Times are given in UTC. Particle number concentrations were taken from the World Data Centre for Aerosols homepage (WDCA, 2014). Temperature and wind direction were provided by the Jungfraujoch station operated by International Foundation High Altitude Research Stations Jungfraujoch and Gornergrat. Cloud presence was detected by measuring the liquid water content using a Particulate Volume Monitor (PVM-100, Gerber Scientific, Reston, VA, USA) and a Cloud Droplet Probe (Droplet Measurement Technologies, Boulder, CO, USA). Sampling phases are marked by colored bars. Homogeneous time periods with particle sampling times are marked.

ACPD
14, 23027–23073, 2014

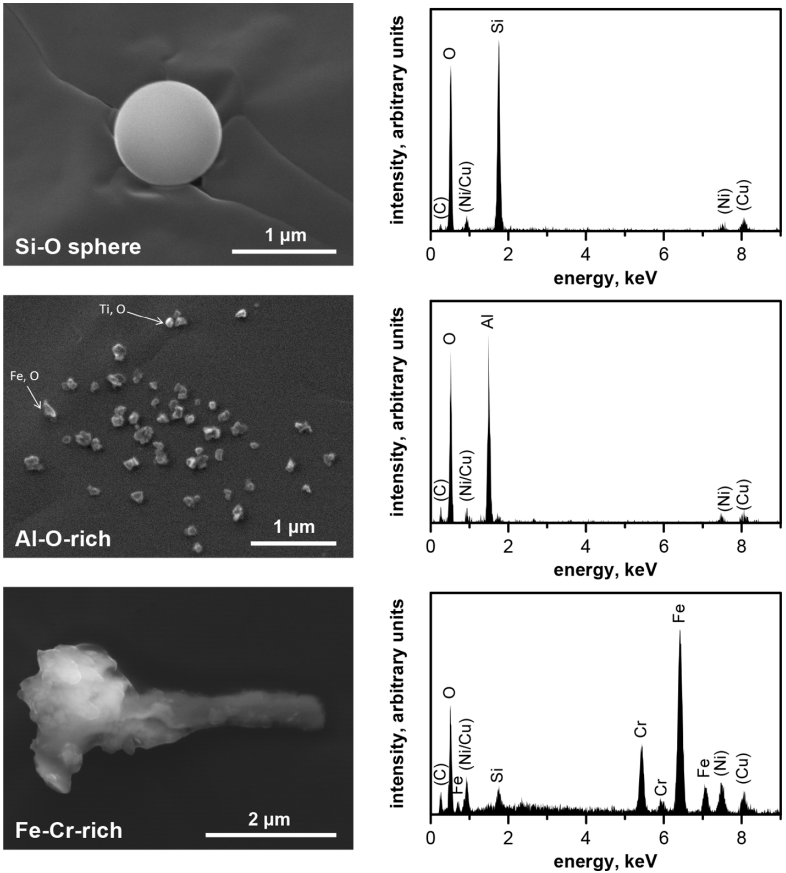

Figure 2. Secondary electron images of contamination artifact particles and according energy-dispersive X-ray spectra with characteristic X-ray peaks of elements marked. Elements contained in the sample substrate are given in parentheses.

ACPD
14, 23027–23073, 2014

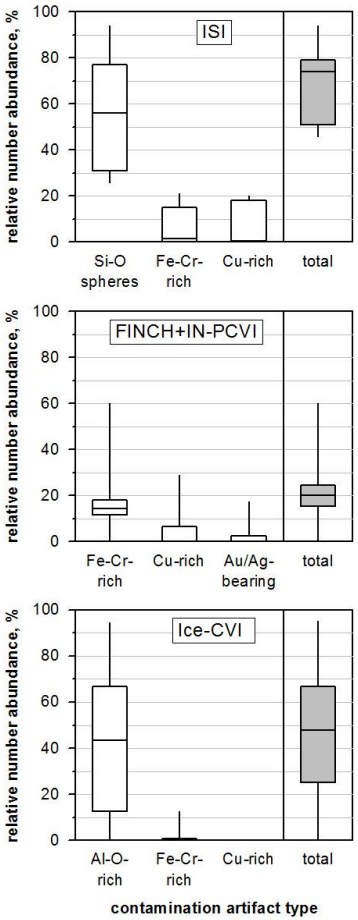

Figure 3. Box-plots of the different contamination artifact particles for each sampling device (top: ISI, middle: FINCH + IN-PCVI, bottom: Ice-CVI). Shown are minimum, lower quartile, median, upper quartile, and maximum.

ACPD
14, 23027–23073, 2014

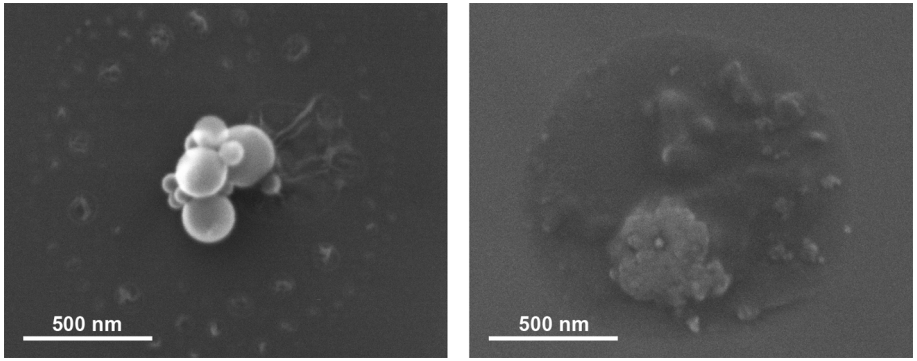

Figure 4. Secondary electron images of droplets with their typical morphology of a halo around a residue.

ACPD
14, 23027–23073, 2014

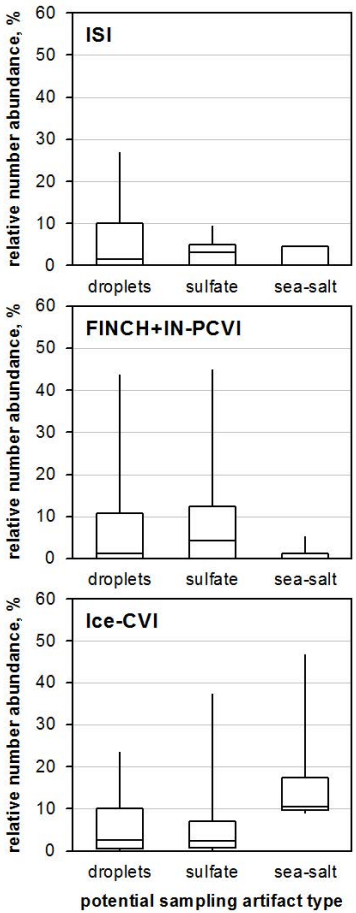

Figure 5. Box-plots of impacted droplet and non-droplet sulfate, sea-salt, and secondary aerosol abundance for ISI, FINCH + IN-PCVI and Ice-CVI. Shown are the minimum, lower quartile, median, upper quartile, and maximum.

ACPD
14, 23027–23073, 2014

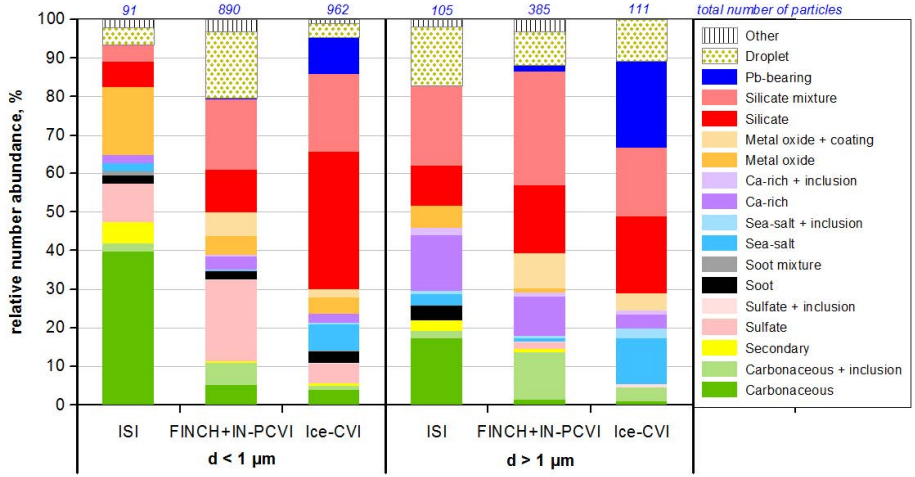

Figure 6. Relative number abundance (all samples) of different particle groups, separately for ISI, FINCH + IN-PCVI and Ice-CVI as well as for supermicron and submicron INP/IPR. The total number of analyzed particles is shown above the bars.

ACPD
14, 23027–23073, 2014

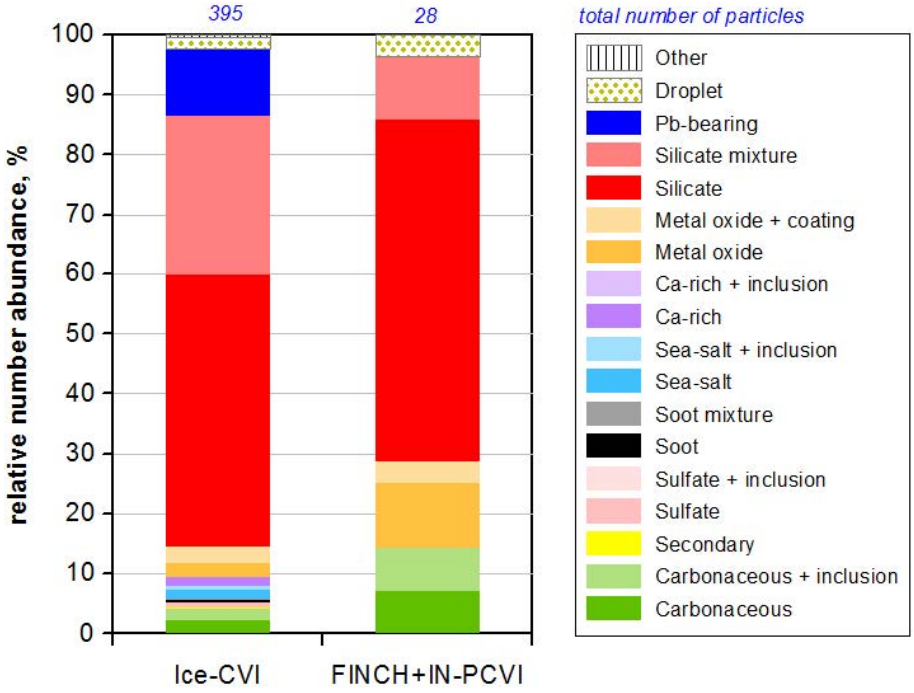

Figure 7. Relative number abundance of different particle groups among INP/IPR for 2 February as determined by FINCH + IN-PCVI and Ice-CVI.

ACPD
14, 23027–23073, 2014

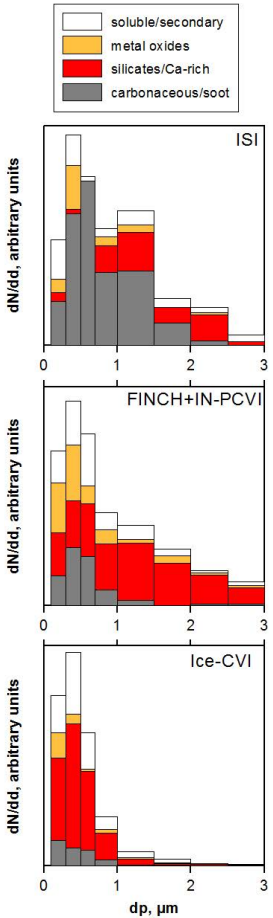

Figure 8. Size distribution of relative abundance of major INP/IPR components for ISI, FINCH + IN-PCVI and Ice-CVI. Particle groups were combined according to potential sources to obtain a sufficient number of particles in each size interval.

ACPD
14, 23027–23073, 2014

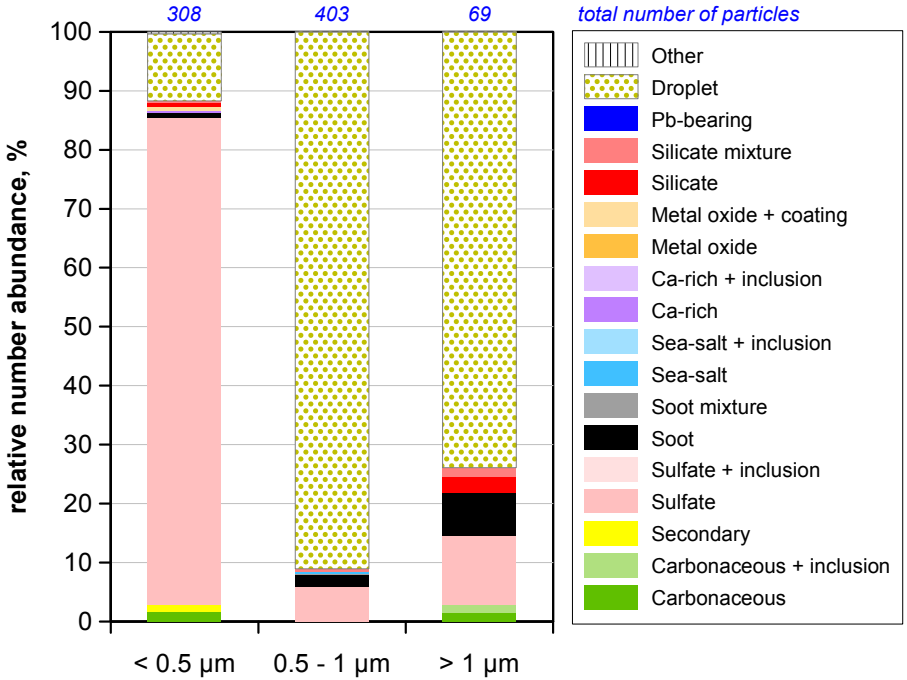

Figure 9. Composition (relative number abundance of different particle groups) of the total aerosol as a function of particle size.

ACPD
14, 23027–23073, 2014

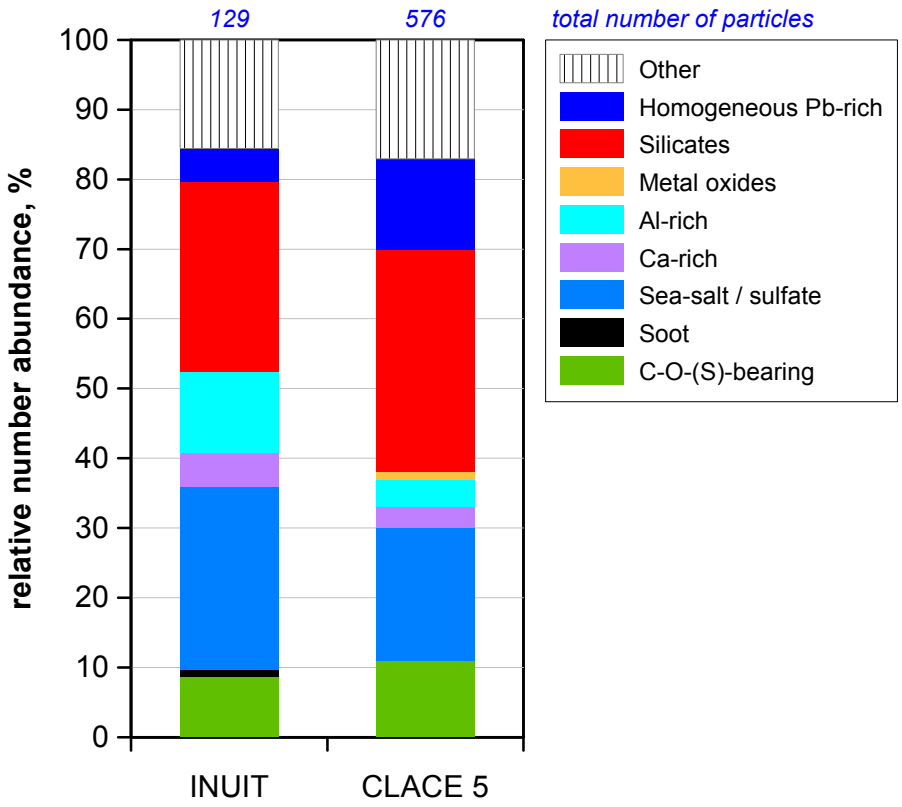

Figure 10. Comparison of the composition/mixing state of Pb-bearing particles from INUIT and CLACE 5.

ACPD
14, 23027–23073, 2014

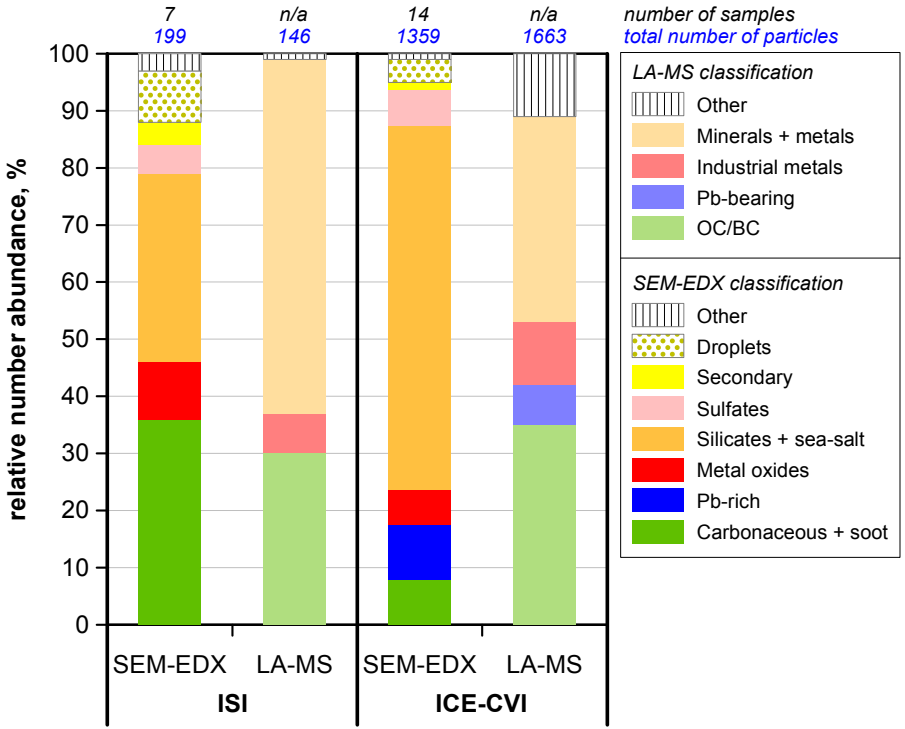

Figure 11. Comparison of particle class abundance determined by SEM-EDX and LA-MS for IPR sampled by ISI and Ice-CVI. To allow for a comparison of the different analytical approaches of SEM-EDX and LA-MS, classes were combined accordingly.

ACPD
14, 23027–23073, 2014